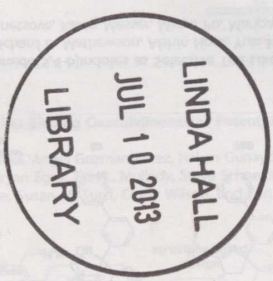
LINDA HALL
JUL 10 2013
LIBRARY

Journal of
Medicinal
Chemistry

JUNE 13, 2013
VOLUME 56 ISSUE 11

JMCMAR 56(11) 4135–4822 (2013)
ISSN 0022-2623
Registered in the U.S. Patent and Trademark Office

ON THE COVER: Single nucleotide polymorphisms (SNPs) in the fat mass and obesity associated gene fto have been implicated in increased body weight in humans. Small molecules targeting the FTO protein have been proposed as a potential treatment for extreme obesity. Using X-ray crystallography, structures of FTO in complex with inhibitors representing six different inhibitor scaffolds have been determined. The results from these detailed structural investigations will aid further development of potent and selective FTO inhibitors. (Aik, W.; et al. *J. Med. Chem.* **2013**, *56*, 3680−3688)

Perspectives

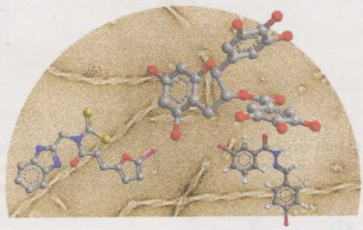

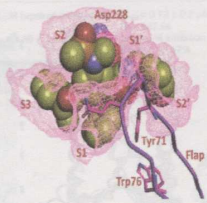

4181 S

dx.doi.org/10.1021/jm3011349

Core Refinement toward Permeable β-Secretase (BACE-1) Inhibitors with Low hERG Activity

Tobias Ginman, Jenny Viklund, Jonas Malmström, Jan Blid, Rikard Emond, Rickard Forsblom, Anh Johansson, Annika Kers, Fredrik Lake, Fernando Sehgelmeble, Karin J. Sterky, Margareta Bergh, Anders Lindgren, Patrik Johansson, Fredrik Jeppsson, Johanna Fälting, Ylva Gravenfors,* and Fredrik Rahm

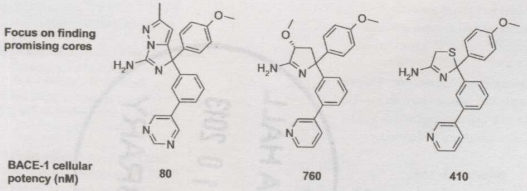

4206

dx.doi.org/10.1021/jm301694x

Identification of Substituted Pyrimido[5,4-*b*]indoles as Selective Toll-Like Receptor 4 Ligands

Michael Chan, Tomoko Hayashi, Richard D. Mathewson, Afshin Nour, Yuki Hayashi, Shiyin Yao, Rommel I. Tawatao, Brian Crain, Igor F. Tsigelny, Valentina L. Kouznetsova, Karen Messer, Minya Pu, Maripat Corr, Dennis A. Carson, and Howard B. Cottam*

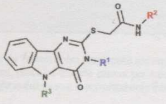

4224

dx.doi.org/10.1021/jm301718c

Structural Optimization, Biological Evaluation, and Application of Peptidomimetic Prostate Specific Antigen Inhibitors

Maya B. Kostova, D. Marc Rosen, Ying Chen, Ronnie C. Mease, and Samuel R. Denmeade*

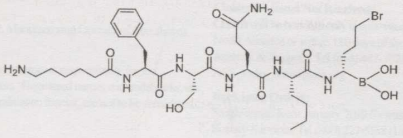

4236 S

dx.doi.org/10.1021/jm400307y

Optimized Method of G-Protein-Coupled Receptor Homology Modeling: Its Application to the Discovery of Novel CXCR7 Ligands

Yasushi Yoshikawa, Shinya Oishi, Tatsuhiko Kubo, Noriko Tanahara, Nobutaka Fujii, and Toshio Furuya*

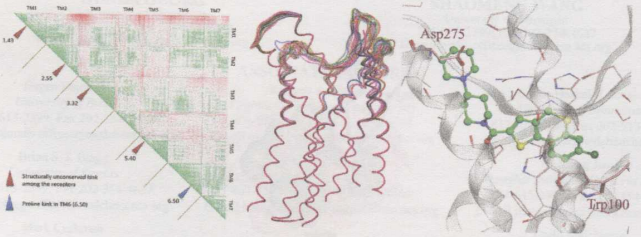

4252 S

dx.doi.org/10.1021/jm400446b

Monitoring Conformational Changes in Peroxisome Proliferator-Activated Receptor α by a Genetically Encoded Photoamino Acid, Cross-Linking, and Mass Spectrometry

Rico Schwarz, Dirk Tänzler, Christian H. Ihling, Mathias Q. Müller, Knut Kölbel, and Andrea Sinz*

4264 S

dx.doi.org/10.1021/jm301886t

Bispyrimidines as Potent Histamine H_4 Receptor Ligands: Delineation of Structure–Activity Relationships and Detailed H_4 Receptor Binding Mode

Harald Engelhardt, Sabine Schultes, Chris de Graaf, Saskia Nijmeijer, Henry F. Vischer, Obbe P. Zuiderveld, Julia Dobler, Katharina Stachurski, Moriz Mayer, Heribert Arnhof, Dirk Scharn, Eric E. J. Haaksma, Iwan J. P. de Esch, and Rob Leurs*

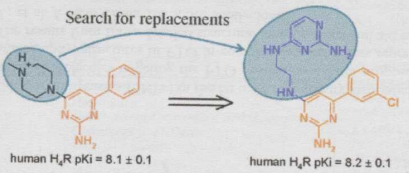

4277 S dx.doi.org/10.1021/jm301905a

Synthesis, Pharmacological Characterization, and Docking Analysis of a Novel Family of Diarylisoxazoles as Highly Selective Cyclooxygenase-1 (COX-1) Inhibitors

Paola Vitale, Stefania Tacconelli, Maria Grazia Perrone, Paola Malerba, Laura Simone, Antonio Scilimati,* Antonio Lavecchia,* Melania Dovizio, Emanuela Marcantoni, Annalisa Bruno, and Paola Patrignani*

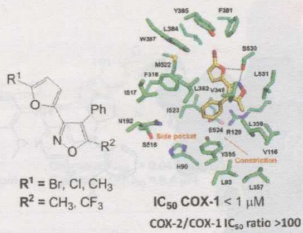

4300 S dx.doi.org/10.1021/jm301910a

Development of Oleanane-Type Triterpenes as a New Class of HCV Entry Inhibitors

Fei Yu, Qi Wang, Zhen Zhang, Yiyun Peng, Yunyan Qiu, Yongying Shi, Yongxiang Zheng, Sulong Xiao,* Han Wang, Xiaoxi Huang, Linyi Zhu, Kunbo Chen, Chuanke Zhao, Chuanling Zhang, Maorong Yu, Dian Sun, Lihe Zhang, and Demin Zhou*

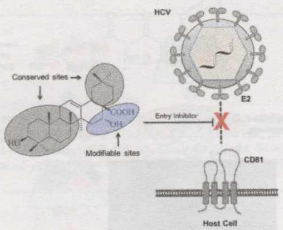

4320 S dx.doi.org/10.1021/jm4000038

Discovery of Novel, Induced-Pocket Binding Oxazolidinones as Potent, Selective, and Orally Bioavailable Tankyrase Inhibitors

Howard Bregman,* Nagasree Chakka, Angel Guzman-Perez, Hakan Gunaydin, Yan Gu, Xin Huang, Virginia Berry, Jingzhou Liu, Yohannes Teffera, Liyue Huang, Bryan Egge, Erin L. Mullady, Steve Schneider, Paul S. Andrews, Ankita Mishra, John Newcomb, Randy Serafino, Craig A. Strathdee, Susan M. Turci, Cindy Wilson, and Erin F. DiMauro

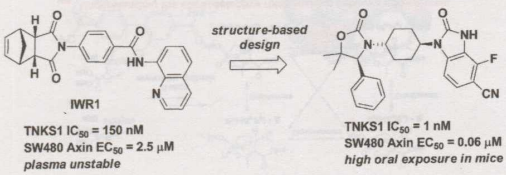

4343
Indazole
(SP6001
Ken-ichi
Yoshio H
Keiji Do
Yoshiyas

4357
Matrix
Yongha

4374
Discove
Moni Sl
Jitendra

4343 S

dx.doi.org/10.1021/jm4000215

Indazole-Based Potent and Cell-Active Mps1 Kinase Inhibitors: Rational Design from Pan-Kinase Inhibitor Anthrapyrazolone (SP600125)

Ken-ichi Kusakabe,* Nobuyuki Ide, Yataro Daigo, Yuki Tachibana, Takeshi, Itoh, Takahiko Yamamoto, Hiroshi Hashizume, Yoshio Hato, Kenichi Higashino, Yousuke Okano, Yuji Sato, Makiko Inoue, Motofumi Iguchi, Takayuki Kanazawa, Yukichi Ishioka, Keiji Dohi, Yasuto Kido, Shingo Sakamoto, Kazuya Yasuo, Masahiro Maeda, Masayo Higaki, Kazuo Ueda, Hidenori Yoshizawa, Yoshiyasu Baba, Takeshi Shiota, Hitoshi Murai, and Yusuke Nakamura

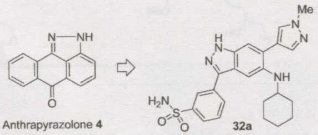

Anthrapyrazolone **4**

Mps1 IC_{50} = 98 nM

32a

Mps1 IC_{50} = 10.4 nM
Cellular Mps1 IC_{50} = 20.5 nM
A549 IC_{50} = 152 nM

4357

dx.doi.org/10.1021/jm400529f

Matrix Metalloproteinase Inhibitors Based on the 3-Mercaptopyrrolidine Core

Yonghao Jin, Mark D. Roycik, Dale B. Bosco, Qiang Cao, Manuel H. Constantino, Martin A. Schwartz, and Qing-Xiang Amy Sang*

4374 S

dx.doi.org/10.1021/jm400053v

Discovery of a New Class of Natural Product-Inspired Quinazolinone Hybrid as Potent Antileishmanial agents

Moni Sharma, Kuldeep Chauhan, Rahul Shivahare, Preeti Vishwakarma, Manish K. Suthar, Abhisheak Sharma, Suman Gupta, Jitendra K. Saxena, Jawahar Lal, Preeti Chandra, Brijesh Kumar, and Prem M. S. Chauhan*

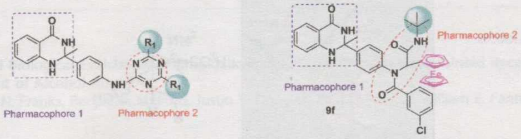

8a;R_1= piperidine, IC_{50}= 3.95 ± 0.8 μM (against amastigote)
SI =101.26
8g;R_1= tetrahydroisoquinoline, IC_{50} = 4.39 ± 1.4 μM,
SI > 91.12
In vivo % inhibition against *L. donovani*/hamster model
8a; 73.15 ± 12.69,
8g; 80.93 ± 10.50

IC_{50} = 0.73 ± 0.2 μM (against amastigote)
SI > 547.94
In vivo % inhibition against *L. donovani*/hamster model
51.42 ± 15.67%

Millefosine; IC_{50}= 8.4 ± 2.1 μM, SI = 1.48

4393 S

dx.doi.org/10.1021/jm4000787

Enantioselective Inhibition of Microbial Lipolytic Enzymes by Nonracemic Monocyclic Enolphosphonate Analogues of Cyclophostin

Vanessa Point, Raj K. Malla, Frederic Carrière, Stéphane Canaan, Christopher D. Spilling,* and Jean-François Cavalier*

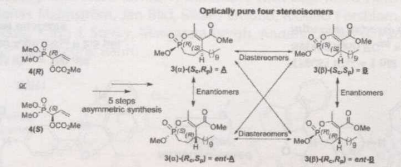

Understanding the stereoselective relationships between non-racemic enolphosphonates and their inhibitory activity towards microbial lipases

4402 S

dx.doi.org/10.1021/jm400080c

Discovery of Novel STAT3 Small Molecule Inhibitors via in Silico Site-Directed Fragment-Based Drug Design

Wenying Yu, Hui Xiao, Jiayuh Lin, and Chenglong Li*

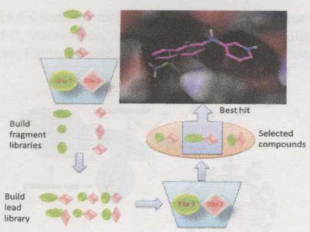

4413 S

dx.doi.org/10.1021/jm4000837

X-ray Crystal Structure of ERK5 (MAPK7) in Complex with a Specific Inhibitor

Jonathan M. Elkins, Jing Wang, Xianming Deng, Michael J. Pattison, J. Simon C. Arthur, Tatiana Erazo, Nestor Gomez, Jose M. Lizcano, Nathanael S. Gray, and Stefan Knapp*

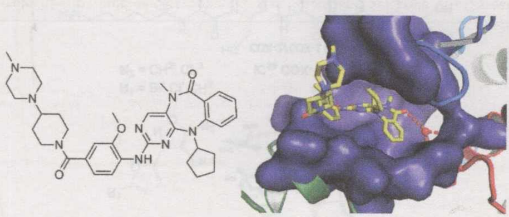

4422 S

dx.doi.org/10.1021/jm400086g

Design, Synthesis, and Molecular Modeling of Novel Pyrido[2,3-*d*]pyrimidine Analogues As Antifolates; Application of Buchwald–Hartwig Aminations of Heterocycles

Aleem Gangjee,* Ojas A. Namjoshi, Sudhir Raghavan, Sherry F. Queener, Roy L. Kisliuk, and Vivian Cody

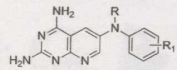

4442 S

dx.doi.org/10.1021/jm4000165

Synthesis and Pharmacological Characterization of 4-Substituted-2-Aminobicyclo[3.1.0]hexane-2,6-dicarboxylates: Identification of New Potent and Selective Metabotropic Glutamate 2/3 Receptor Agonists

James A. Monn,* Matthew J. Valli, Steven M. Massey, Junliang Hao, Matthew R. Reinhard, Mark G. Bures, Beverly A. Heinz, Xushan Wang, Joan H. Carter, Brian G. Getman, Gregory A. Stephenson, Marc Herin, John T. Catlow, Steven Swanson, Bryan G. Johnson, David L. McKinzie, and Steven S. Henry

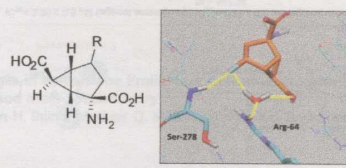

4456 S

dx.doi.org/10.1021/jm400115k

Design, Synthesis, and Inhibitory Activity of Potent, Photoswitchable Mast Cell Activation Inhibitors

Willem A. Velema, Marco van der Toorn, Wiktor Szymanski,* and Ben L. Feringa*

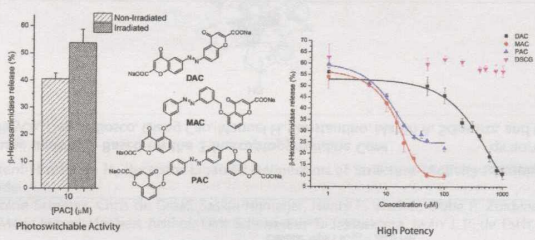

4465 dx.doi.org/10.1021/jm400138z

Discovery of Potent, Selective Chymase Inhibitors via Fragment Linking Strategies

Steven J. Taylor,* Anil K. Padyana, Asitha Abeywardane, Shuang Liang, Ming-Hong Hao, Stéphane De Lombaert, John Proudfoot, Bennett S. Farmer III, Xiang Li, Brandon Collins, Leslie Martin, Daniel R. Albaugh, Melissa Hill-Drzewi, Steven S. Pullen, and Hidenori Takahashi

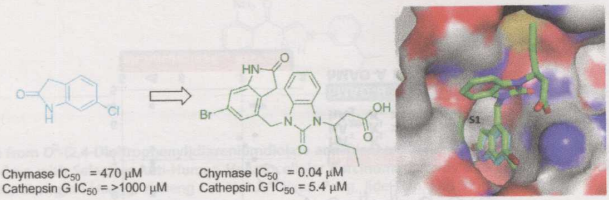

4482 S dx.doi.org/10.1021/jm400182t

Discovery of 7-Oxopyrazolo[1,5-*a*]pyrimidine-6-carboxamides as Potent and Selective CB_2 Cannabinoid Receptor Inverse Agonists

Mojgan Aghazadeh Tabrizi,* Pier Giovanni Baraldi,* Giulia Saponaro, Allan R. Moorman, Romeo Romagnoli, Delia Preti, Stefania Baraldi, Emanuela Ruggiero, Cristina Tintori, Tiziano Tuccinardi, Fabrizio Vincenzi, Pier Andrea Borea, and Katia Varani

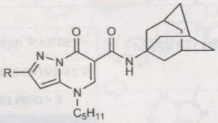

R = Ph: hK_i CB_2 = 2.5 nM, hK_i CB_1> 10000 nM, SI > 3906
R = 2-CH_3-Ph: hK_i CB_2 = 2.8 nM, hK_i CB_1> 10000 nM, SI > 3496
R = 4-Cl-Ph: hK_i CB_2 = 3.8 nM, hK_i CB_1> 10000 nM, SI > 2597
R = Furan-2-yl: hK_i CB_2 = 4.9 nM, hK_i CB_1> 10000 nM, SI > 2032

4497 S dx.doi.org/10.1021/jm400211f

Fragment-Based Ligand Design of Novel Potent Inhibitors of Tankyrases

E. Andreas Larsson,* Anna Jansson, Fui Mee Ng, Siew Wen Then, Resmi Panicker, Boping Liu, Kanda Sangthongpitag, Vishal Pendharkar, Shi Jing Tai, Jeffrey Hill, Chen Dan, Soo Yei Ho, Wei Wen Cheong, Anders Poulsen, Stephanie Blanchard, Grace Ruiting Lin, Jenefer Alam, Thomas H. Keller, and Pär Nordlund*

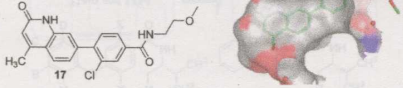

4509 S

dx.doi.org/10.1021/jm400257a

Synthesis, ^{18}F-Radiolabeling, and in Vivo Biodistribution Studies of *N*-Fluorohydroxybutyl Isatin Sulfonamides using Positron Emission Tomography

Panupun Limpachayaporn, Stefan Wagner, Klaus Kopka, Sven Hermann, Michael Schäfers, and Günter Haufe*

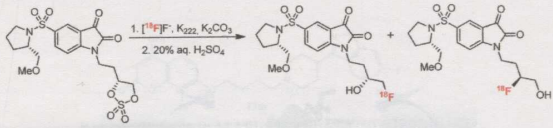

4521 S

dx.doi.org/10.1021/jm400266t

Lead Optimization of a 4-Aminopyridine Benzamide Scaffold To Identify Potent, Selective, and Orally Bioavailable TYK2 Inhibitors

Jun Liang,* Anne van Abbema, Mercedesz Balazs, Kathy Barrett, Leo Berezhkovsky, Wade Blair, Christine Chang, Donnie Delarosa, Jason DeVoss, Jim Driscoll, Charles Eigenbrot, Nico Ghilardi, Paul Gibbons, Jason Halladay, Adam Johnson, Pawan Bir Kohli, Yingjie Lai, Yanzhou Liu, Joseph Lyssikatos, Priscilla Mantik, Kapil Menghrajani, Jeremy Murray, Ivan Peng, Amy Sambrone, Steven Shia, Young Shin, Jan Smith, Sue Sohn, Vickie Tsui, Mark Ultsch, Lawren C. Wu, Yisong Xiao, Wenqian Yang, Judy Young, Birong Zhang, Bing-yan Zhu, and Steven Magnuson

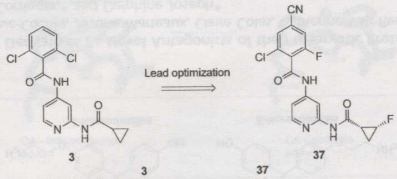

	3	37
TYK2 Ki (nM)	4.8	1.6
JAK1-index	17x	60x
JAK2-index	6x	39x
JAK3-index	53x	239x

4537 S

dx.doi.org/10.1021/jm400268b

Design, Synthesis, and Biological Evaluation of Aminoalkylindole Derivatives as Cannabinoid Receptor Ligands with Potential for Treatment of Alcohol Abuse

Tamara Vasiljevik, Lirit N. Franks, Benjamin M. Ford, Justin T. Douglas, Paul L. Prather, William E. Fantegrossi, and Thomas E. Prisinzano*

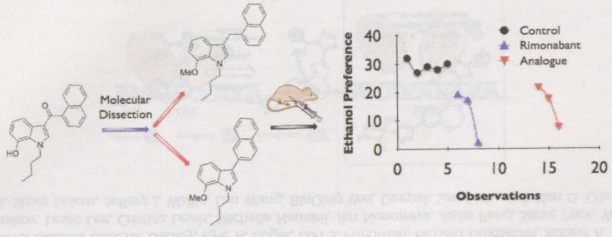

4551 S

dx.doi.org/10.1021/jm400275h

Discovery of *N*-{4-[(3-Hydroxyphenyl)-3-methylpiperazin-1-yl]methyl-2-methylpropyl}-4-phenoxybenzamide Analogues as Selective Kappa Opioid Receptor Antagonists

Chad M. Kormos, Chunyang Jin, Juan Pablo Cueva, Scott P. Runyon, James B. Thomas, Lawrence E. Brieaddy, S. Wayne Mascarella, Hernán A. Navarro, Brian P. Gilmour, and F. Ivy Carroll*

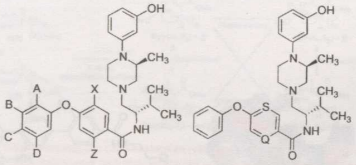

11a-q and **12a-l**

13, Q = N, S = CH
14, Q = CH, S = N

4568 S

dx.doi.org/10.1021/jm400312y

Design and Selection Parameters to Accelerate the Discovery of Novel Central Nervous System Positron Emission Tomography (PET) Ligands and Their Application in the Development of a Novel Phosphodiesterase 2A PET Ligand

Lei Zhang,* Anabella Villalobos, Elizabeth M. Beck, Thomas Bocan, Thomas A. Chappie, Laigao Chen, Sarah Grimwood, Steven D. Heck, Christopher J. Helal, Xinjun Hou, John M. Humphrey, Jiemin Lu, Marc B. Skaddan, Timothy J. McCarthy, Patrick R. Verhoest, Travis T. Wager, and Kenneth Zasadny

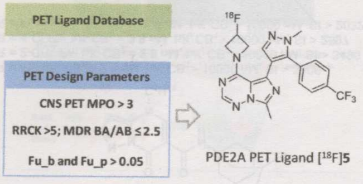

PDE2A PET Ligand [^{18}F]**5**

4580 S

dx.doi.org/10.1021/jm400336x

Dual Targeting of Adenosine A_{2A} Receptors and Monoamine Oxidase B by 4*H*-3,1-Benzothiazin-4-ones

Anne Stößel, Miriam Schlenk, Sonja Hinz, Petra Küppers, Jag Heer, Michael Gütschow,* and Christa E. Müller*

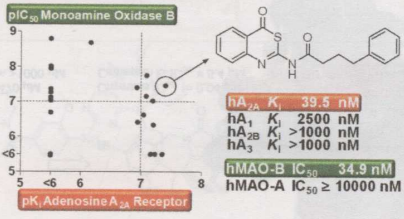

4597

dx.doi.org/10.1021/jm4003632

Discovery of 2-{3-[2-(1-Isopropyl-3-methyl-1*H*-1,2−4-triazol-5-yl)-5,6-dihydrobenzo[*f*]imidazo[1,2-*d*][1,4]oxazepin-9-yl]-1*H*-pyrazol-1-yl}-2-methylpropanamide (GDC-0032): A β-Sparing Phosphoinositide 3-Kinase Inhibitor with High Unbound Exposure and Robust in Vivo Antitumor Activity

Chudi O. Ndubaku,* Timothy P. Heffron,* Steven T. Staben, Matthew Baumgardner, Nicole Blaquiere, Erin Bradley, Richard Bull, Steven Do, Jennafer Dotson, Danette Dudley, Kyle A. Edgar, Lori S. Friedman, Richard Goldsmith, Robert A. Heald, Aleksandr Kolesnikov, Leslie Lee, Cristina Lewis, Michelle Nannini, Jim Nonomiya, Jodie Pang, Steve Price, Wei Wei Prior, Laurent Salphati, Steve Sideris, Jeffery J. Wallin, Lan Wang, BinQing Wei, Deepak Sampath, and Alan G. Olivero

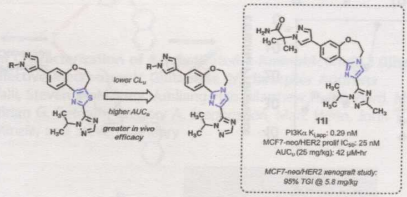

4611

dx.doi.org/10.1021/jm400364h

Synthesis of Mixed (*E*,*Z*)-, (*E*)-, and (*Z*)-Norendoxifen with Dual Aromatase Inhibitory and Estrogen Receptor Modulatory Activities

Wei Lv, Jinzhong Liu, Deshun Lu, David A. Flockhart, and Mark Cushman*

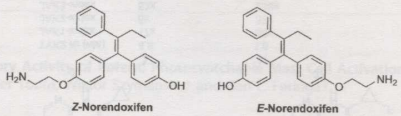

4619

dx.doi.org/10.1021/jm400374q

Identification of Cinnamic Acid Derivatives As Novel Antagonists of the Prokaryotic Proton-Gated Ion Channel GLIC

Marie S. Prevost, Sandrine Delarue-Cochin, Justine Marteaux, Claire Colas, Catherine Van Renterghem, Arnaud Blondel, Thérèse Malliavin,* Pierre-Jean Corringer,* and Delphine Joseph*

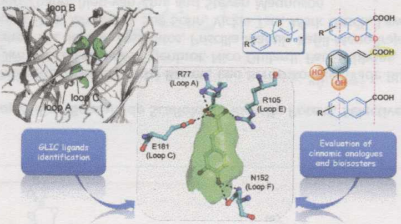

4631 S dx.doi.org/10.1021/jm4003928

1-Phenyl-4-benzoyl-1*H*-1,2,3-triazoles as Orally Bioavailable Transcriptional Function Suppressors of Estrogen-Related Receptor α

Shilin Xu, Xiaoxi Zhuang, Xiaofen Pan, Zhang Zhang, Lei Duan, Yingxue Liu, Lianwen Zhang, Xiaomei Ren,* and Ke Ding*

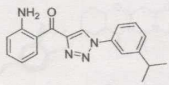

4641 S dx.doi.org/10.1021/jm400393u

Hybrid Molecule from O^2-(2,4-Dinitrophenyl)diazeniumdiolate and Oleanolic Acid: A Glutathione *S*-Transferase π-Activated Nitric Oxide Prodrug with Selective Anti-Human Hepatocellular Carcinoma Activity and Improved Stability

Junjie Fu, Ling Liu, Zhangjian Huang, Yisheng Lai, Hui Ji,* Sixun Peng, Jide Tian, and Yihua Zhang*

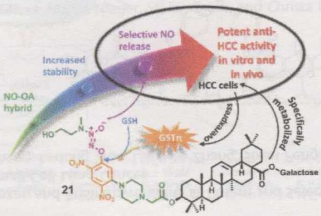

4656 dx.doi.org/10.1021/jm400404v

CROSS: An Efficient Workflow for Reaction-Driven Rescaffolding and Side-Chain Optimization Using Robust Chemical Reactions and Available Reagents

Andreas Evers,* Gerhard Hessler, Li-hsing Wang, Simon Werrel, Peter Monecke, and Hans Matter

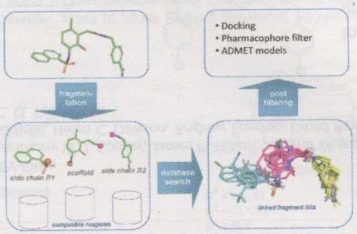

4671
Synthe
Antips
Yin Ch
Guiser

4691
Xanth
Fabriz

4701
Bindi
Modu
Franc
Ettore

4671 dx.doi.org/10.1021/jm400408r

Synthesis and Biological Investigation of Coumarin Piperazine (Piperidine) Derivatives as Potential Multireceptor Atypical Antipsychotics

Yin Chen, Songlin Wang, Xiangqing Xu, Xin Liu, Minquan Yu, Song Zhao, Shicheng Liu, Yinli Qiu, Tan Zhang, Bi-Feng Liu, and Guisen Zhang*

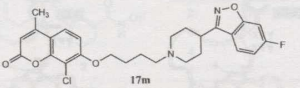

17m

In *vitro* (K_i, nM): D_2, 2.6; D_3, 4.3; 5-HT_{1A}, 3.3; 5-HT_{2A}, 0.3; 5-HT_{2C}, 1700.7; H_1, 1125.3
In *vivo* (ED_{50}, mg/kg): APO, 0.14; MK-801, 0.32; CAR, 6.50; CAT, 70.85
Pharmacokinetic: $t_{1/2}$, 6.7h; F%, 32

4691 dx.doi.org/10.1021/jm400414j

Xanthates and Trithiocarbonates Strongly Inhibit Carbonic Anhydrases and Show Antiglaucoma Effects in Vivo

Fabrizio Carta, Atilla Akdemir, Andrea Scozzafava, Emanuela Masini, and Claudiu T. Supuran*

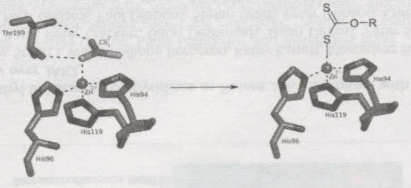

CA - trithiocarbonate adduct

CA - xanthate adduct

4701 dx.doi.org/10.1021/jm400419e

Binding Mechanism of the Farnesoid X Receptor Marine Antagonist Suvanine Reveals a Strategy To Forestall Drug Modulation on Nuclear Receptors. Design, Synthesis, and Biological Evaluation of Novel Ligands

Francesco Saverio Di Leva, Carmen Festa, Claudio D'Amore, Simona De Marino, Barbara Renga, Maria Valeria D'Auria, Ettore Novellino, Vittorio Limongelli,* Angela Zampella,* and Stefano Fiorucci*

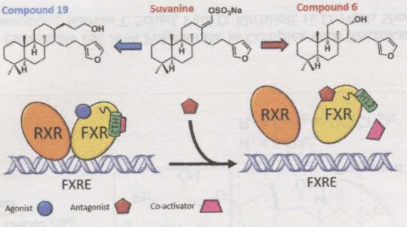

4718 S

dx.doi.org/10.1021/jm400435a

1,4-Benzothiazine ATP-Sensitive Potassium Channel Openers: Modifications at the C-2 and C-6 Positions

Alma Martelli, Giuseppe Manfroni,* Paola Sabbatini, Maria Letizia Barreca, Lara Testai, Michela Novelli, Stefano Sabatini, Serena Massari, Oriana Tabarrini, Pellegrino Masiello, Vincenzo Calderone,* and Violetta Cecchetti

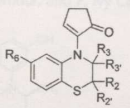

R_2, $R_{2'}$, R_3, $R_{3'}$ = H, Me

R_6 = H, Me, $SO_2N(i\text{-}Bu)_2$, Ac, Et, NH_2, NHAc

4729 S

dx.doi.org/10.1021/jm400458q

Optimized Chemical Probes for REV-ERBα

Ryan P. Trump,* Stefano Bresciani, Anthony W. J. Cooper, James P. Tellam, Justyna Wojno, John Blaikley, Lisa A. Orband-Miller, Jennifer A. Kashatus, Mohamed Boudjelal, Helen C. Dawson, Andrew Loudon, David Ray, Daniel Grant, Stuart N. Farrow, Timothy M. Willson, and Nicholas C. O. Tomkinson

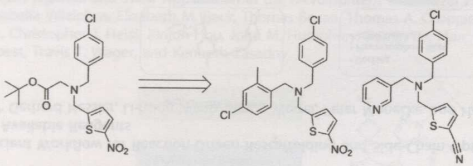

In vivo probes with improved potency and selectivity for REV-ERBα

4738 S

dx.doi.org/10.1021/jm400463q

Novel Hybrids of (Phenylsulfonyl)furoxan and Anilinopyrimidine as Potent and Selective Epidermal Growth Factor Receptor Inhibitors for Intervention of Non-Small-Cell Lung Cancer

Chun Han, Zhangjian Huang, Chao Zheng, Ledong Wan, Lianwen Zhang, Sixun Peng, Ke Ding,* Hongbin Ji,* Jide Tian, and Yihua Zhang*

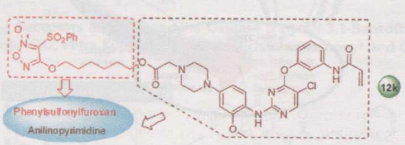

4749 S

dx.doi.org/10.1021/jm400479p

Dual-Functional *abeo*-Taxane Derivatives Destabilizing Microtubule Equilibrium and Inhibiting NF-κB Activation

Yu Zhao, Jia Su, Masuo Goto, Susan L. Morris-Natschke, Yan Li, Qin-Shi Zhao,* Zhu-Jun Yao,* and Kuo-Hsiung Lee*

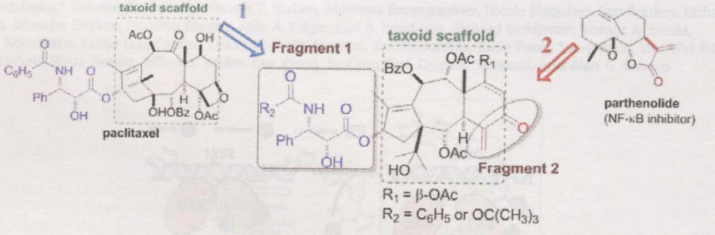

4758 S

dx.doi.org/10.1021/jm4004889

X-ray Crystal Structures of the *Escherichia coli* RNA Polymerase in Complex with Benzoxazinorifamycins

Vadim Molodtsov, Irosha N. Nawarathne, Nathan T. Scharf, Paul D. Kirchhoff, H. D. Hollis Showalter, George A. Garcia, and Katsuhiko S. Murakami*

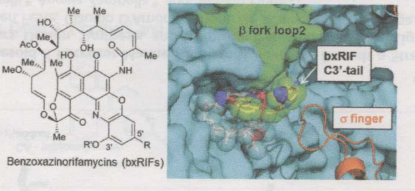

4764 S

dx.doi.org/10.1021/jm4004895

Identification of *C*-2 Hydroxyethyl Imidazopyrrolopyridines as Potent JAK1 Inhibitors with Favorable Physicochemical Properties and High Selectivity over JAK2

Mark Zak,* Christopher A. Hurley, Stuart I. Ward, Philippe Bergeron, Kathy Barrett, Mercedesz Balazs, Wade S. Blair, Richard Bull, Paroma Chakravarty, Christine Chang, Peter Crackett, Gauri Deshmukh, Jason DeVoss, Peter S. Dragovich, Charles Eigenbrot, Charles Ellwood, Simon Gaines, Nico Ghilardi, Paul Gibbons, Stefan Gradl, Peter Gribling, Chris Hamman, Eric Harstad, Peter Hewitt, Adam Johnson, Tony Johnson, Jane R. Kenny, Michael F. T. Koehler, Pawan Bir Kohli, Sharada Labadie, Wyne P. Lee, Jiangpeng Liao, Marya Liimatta, Rohan Mendonca, Raman Narukulla, Rebecca Pulk, Austin Reeve, Scott Savage, Steven Shia, Micah Steffek, Savita Ubhayakar, Anne van Abbema, Ignacio Aliagas, Barbara Avitabile-Woo, Yisong Xiao, Jing Yang, and Janusz J. Kulagowski

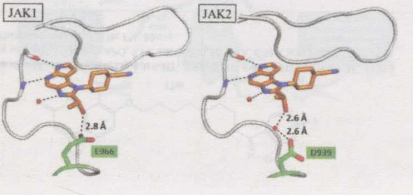

4786 dx.doi.org/10.1021/jm4005048

Structure–Activity Relationship of N,N′-Disubstituted Pyrimidinetriones as $Ca_V1.3$ Calcium Channel-Selective Antagonists for Parkinson's Disease

Soosung Kang, Garry Cooper, Sara Fernandez Dunne, Chi-Hao Luan, D. James Surmeier, and Richard B. Silverman*

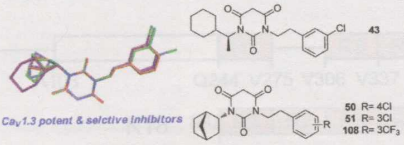

4798 dx.doi.org/10.1021/jm4005175

Antagonists for the Orphan G-Protein-Coupled Receptor GPR55 Based on a Coumarin Scaffold

Viktor Rempel, Nicole Volz, Franziska Gläser, Martin Nieger, Stefan Bräse, and Christa E. Müller*

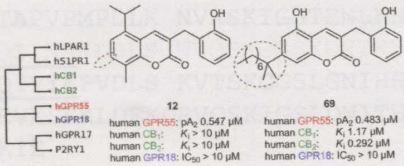

Brief Articles

4811 dx.doi.org/10.1021/jm400246e

Quinolin-4(1*H*)-imines are Potent Antiplasmodial Drugs Targeting the Liver Stage of Malaria

Tiago Rodrigues,* Filipa P. da Cruz, Maria J. Lafuente-Monasterio, Daniel Gonçalves, Ana S. Ressurreição, Ana R. Sitoe, Maria R. Bronze, Jiri Gut, Gisbert Schneider, Maria M. Mota, Philip J. Rosenthal, Miguel Prudêncio, Francisco-Javier Gamo, Francisca Lopes, and Rui Moreira

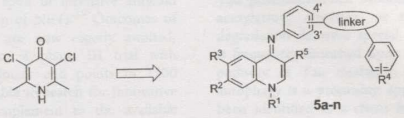

R^1 = Me, Et
R^2 = Cl, CF_3
R^3 = H, F
R^4 = H, Cl, CF_3, OCF_3
R^5 = H, CO_2Et
Linker = O, CH_2, CH_2CH_2

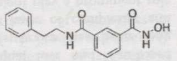

3

HDAC	Class	IC_{50} (μM)
2	I	9.0
8	I	0.12
4	IIa	>33
6	IIb	0.036

Additions and Corrections

Ⓢ Supporting Information available via online article

Journal of
Medicinal Chemistry

Journal of Medicinal Chemistry (ISSN 0022-2623) is published semimonthly by the American Chemical Society at 1155 16th St. NW, Washington, DC 20036. Periodicals postage paid at Washington, DC and additional mailing offices.

POSTMASTER: Send address changes to Journal of Medicinal Chemistry, Subscription Services, P.O. Box 3337, Columbus, OH 43210.

structions for Authors and the ACS Journal Publishing Agreement:
sit the ACS Web site (http://paragonplus.acs.org/login). Please conform to these structions when submitting manuscripts.

anuscript Submission:
bmit via the Journal Web site (http://pubs.acs.org/journal/jmcmar).

cepted Papers and Proofs:
rect correspondence to Journal Production & Manufacturing Operations (see above).

urnal Policies:
e American Chemical Society and its Editors assume no responsibility for the tements and opinions advanced by contributors. Registered names and trademarks, etc., ed in this publication, even without specific indication thereof, are not to be considered protected by law.

ange of E-mail or Mailing Address:
r members only, notify Subscription Services (see above). Include both old and new dresses.

w and Renewal Subscriptions:
mbers send payment to American Chemical Society, P.O. Box 182426, Columbus, H 43218-2426. Institutions send payment to American Chemical Society, P.O. Box 2977, Columbus, OH 43218-2977.

13 Subscription and Ordering Information:
'S members may purchase a Web subscription for $90. Contact Member Services (see ove). Institutional subscribers may contact Sales Analysis & Support (see above) for eb and print subscription information.

Digital Object Identifier (DOI):
The DOI identification system for digital media has been designed to provide persistent and reliable identification of digital objects. Information on the DOI and its governing body, the International DOI Foundation, can be found at http://www.doi.org. The DOI is prominently displayed on each published paper.

Claims for Issues Not Received:
Claims will be honored only if submitted within 90 days of the issue date for subscribers in North America or within 180 days of the issue date for all other subscribers. Contact Sales Analysis & Support. Tel (614) 447-3674 or (888) 338-0012; Fax (614) 447-5475; E-mail ACS_Pubs_Assist@acs.org.

Back Issue Orders:
Single issues from January 2010 forward are available for a fee from the Office of Society Services. Tel (800) 227-5558 (US); (202) 872-4600 (worldwide); Fax (202) 872-6067; E-mail help@acs.org.

Bulk Reprint Orders:
For information on ordering reprints, see the specific article on http://pubs.acs.org or instructions at http://pubs.acs.org/page/copyright/permissions.html or contact Cierant Corporation at (866)-305-0111 9am to 5pm EST.

Supporting Information (SI):
SI from 1995 to present is available free of charge from the journal's home page (http://pubs.acs.org/journal/jmcmar). For information on electronic access, send e-mail to support@services.acs.org. SI prior to 1995 is available for a fee, from Office of Society Services. Tel (800) 227-5558 (US); (202) 872-4600 (worldwide); Fax (202) 872-6067; E-mail help@acs.org.

nadian GST Reg. No. 127571347

Fernan
Institut
Courtn
Univers
Shanka
Univers
Peter B
PhaRm
Maria J
Institut
Giusep
Univers
Carsten
Univers
Li Che
Roche,
Ji-Wan
Nationa
William
Univers
Ke Din
Guangz
and He
Sheng
The Scr
Steven
Abbott
Carlos
Sanofi
Jason E
Univers
Arun K
Purdue
Michae
Univers
Holger
Heinric
Duesse

Journal of
Medicinal Chemistry

Journal of Medicinal Chemistry

Article

pubs.acs.org/jmc

Synthesis of Mixed (*E*,*Z*)-, (*E*)-, and (*Z*)-Norendoxifen with Dual Aromatase Inhibitory and Estrogen Receptor Modulatory Activities

Wei Lv,[†] Jinzhong Liu,[‡] Deshun Lu,[‡] David A. Flockhart,[‡] and Mark Cushman*[,†]

[†]Department of Medicinal Chemistry and Molecular Pharmacology, College of Pharmacy and The Purdue University Center for Cancer Research, Purdue University, West Lafayette, Indiana 47907, United States

[‡]Division of Clinical Pharmacology, Department of Medicine, Indiana University School of Medicine, Indianapolis, Indiana 46202, United States

ABSTRACT: The first synthesis of the tamoxifen metabolite norendoxifen is reported. This included syntheses of (*E*)-norendoxifen, (*Z*)-norendoxifen, and (*E*,*Z*)-norendoxifen isomers. (*Z*)-Norendoxifen displayed affinity for aromatase (K_i 442 nM), estrogen receptor-α (EC_{50} 17 nM), and estrogen receptor-β (EC_{50} 27.5 nM), while the corresponding values for (*E*)-norendoxifen were aromatase (K_i 48 nM), estrogen receptor-α (EC_{50} 58.7 nM), and estrogen receptor-β (EC_{50} 78.5 nM). Docking and energy minimization studies were performed with (*E*)-norendoxifen on aromatase, and the results provide a foundation for structure-based drug design. The oral pharmacokinetic parameters for (*E*,*Z*)-norendoxifen were determined in mice, and (*Z*)-norendoxifen was found to result in significantly higher plasma concentrations and exposures (AUC values) than (*E*)-norendoxifen. The affinities of both isomers for aromatase and the estrogen receptors, as well as the pharmacokinetic results, support the further development of norendoxifen and its analogues for breast cancer treatment.

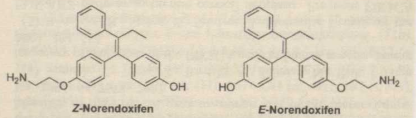

Z-Norendoxifen *E*-Norendoxifen

INTRODUCTION

Breast cancer is the most frequently diagnosed cancer in women, and it is also the second leading cause of cancer-related deaths in women in the United States. It is estimated that 226870 new cases of invasive breast cancer and 63300 new cases of in situ breast cancer occurred among women in the United States in 2012, along with 39510 breast cancer deaths.[1] It has been established that 60% of premenopausal and 75% of postmenopausal breast cancer patients are estrogen receptor (ER) positive, with cancers that are dependent on estrogen for proliferation, making them suitable for hormonal therapy (antiestrogen treatment).[2] The selective estrogen receptor modulator tamoxifen (Figure 1) has been widely used for more than 30 years as the first-line hormonal therapy and adjuvant therapy after surgery for ER-positive breast cancer patients. Tamoxifen blocks ER-stimulated tumor growth in the breast, providing a 47% reduction of recurrence and 26% reduction of mortality as documented in a 5-year treatment clinical trial.[3] Tamoxifen also acts as an ER agonist in bones, uterus, and other tissues, which is beneficial for preventing bone demineralization in postmenopausal women.[4] Although the benefits are prominent, the use of tamoxifen suffers from intrinsic and acquired drug resistance, and it has only been proven to be effective for a maximum of 10 years.[5,6] In postmenopausal women, an alternative strategy to block the effects of estrogen in promoting breast cancer is to use aromatase inhibitors (AIs) to reduce estrogen biosynthesis. Currently, three AIs (letrozole, anastrozole, and exemestane, Figure 1) have been approved for breast cancer treatment. Several clinical trials have demonstrated that the use of AIs is superior to tamoxifen in the treatment of postmenopausal women with ER-positive breast cancer. Generally, compared to tamoxifen, AIs are more effective, with increased disease-free survival, enhanced safety profile, and better tolerability.[7−11] However, the use of AIs is also accompanied by significant side effects, including reduction of the bone density, severe musculoskeletal pain, and increased frequency of cardiovascular and thromboembolic events.[12−16] Most of these side effects of AIs have been attributed to global depletion of estrogen. There has been a need to develop new aromatase inhibitors with novel mechanisms that may cause fewer side effects.

We recently reported the human metabolism of tamoxifen to the potent aromatase inhibitor norendoxifen of undetermined stereochemistry (Figure 1).[17] Norendoxifen competitively inhibits recombinant human aromatase with an IC_{50} of 90 nM. Norendoxifen also shows good selectivity toward aromatase among other CYP450 enzymes, including CYP2B6, 2C9, 2C19, 2D6, and 3A. The high potency and selectivity make norendoxifen an ideal lead compound for developing new therapeutic agents for breast cancer. Two unique features make norendoxifen attractive as a lead compound for the development of new breast cancer chemotherapeutic agents. (1) The close structural relationship of norendoxifen to tamoxifen suggests that it would be possible to make a series of compounds with dual aromatase inhibitory activity and ER modulatory activity. The aromatase inhibitory activity could efficiently block estrogen biosynthesis in the breast to inhibit

Received: March 11, 2013
Published: June 3, 2013

   dx.doi.org/10.1021/jm400418

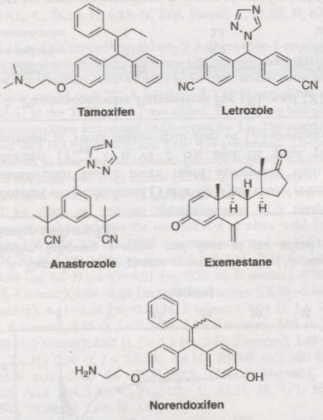

Figure 1. The structures of the selective estrogen receptor modulator tamoxifen, the aromatase inhibitors letrozole, anastrozole, and exemestane, and the tamoxifen metabolite norendoxifen.

the tumor growth, while the estrogen receptor modulatory activity could possibly ameliorate the side effects in bones and other tissues caused by estrogen depletion. In fact, the combination of the aromatase inhibitor anastrozole with the selective estrogen receptor modulator tamoxifen has been reported to result in fewer fractures than when anastrozole was used alone.[18] (2) Because norendoxifen is a metabolite of the widely used drug tamoxifen, many patients have already been exposed to it.

This report documents the first synthesis of (*E*,*Z*)-norendoxifen, as well as the syntheses of (*E*)-norendoxifen (*E*:*Z* > 100:1) and (*Z*)-norendoxifen (*E*:*Z* 1:10). The aromatase inhibitory activity and ER binding affinities for mixed (*E*,*Z*)-, as well as (*E*)- and (*Z*)-norendoxifen, were also evaluated. The possible binding mode of (*E*)-norendoxifen with aromatase was explored by molecular modeling methods. The results of these studies will facilitate future structure-based drug design efforts.

■ RESULTS AND DISCUSSION

Synthesis of Mixed (*E*,*Z*)-, (*E*)-, and (*Z*)-Norendoxifen. The syntheses of 4-hydroxytamoxifen (with a dimethylaminoethoxy side chain) and endoxifen (with a methylaminoethoxy side chain) have previously been reported.[19−21] However, the synthesis of norendoxifen (with an aminoethoxy side chain) has not been reported in the chemical literature. This report describes the first synthesis of norendoxifen via a short and efficient synthetic pathway (Scheme 1). Starting from the 4,4′-dihydroxybenzophenone **1**, the McMurry coupling reaction with propiophenone afforded the diphenol **2** in high yield (88%).[19] The diphenol **2** was then monoalkylated with 2-iodoacetamide in the presence of potassium carbonate to provide the amide **3**. In the last step, the reduction of the amide proceeded well with lithium aluminum hydride to afford norendoxifen **4** in high yield (82%) as a 1:1 mixture of *E*- and *Z*- isomers.

Scheme 1. Synthesis of Mixed (*E*,*Z*)-Norendoxifen 4[a]

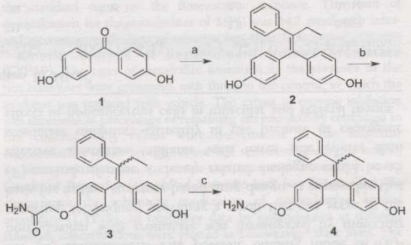

[a]Reagents and conditions: (a) propiophenone, Zn, $TiCl_4$, THF, 88%; (b) ICH_2CONH_2, acetone, K_2CO_3, 45%; (c) LAH, $AlCl_3$, THF, 82%.

The synthesis of mixed (*E*,*Z*)-norendoxifen revealed that the *E*- and *Z*- isomers had strikingly different solubilities in methanol. Trituration of the solid (*E*,*Z*)-norendoxifen with methanol preferentially dissolved the Z isomer, allowing the pure (*E*)-norendoxifen (*E*:*Z* > 100:1) to be filtered off in nearly 40% yield (Scheme 2). The stereochemistry of (*E*)-norendox-

Scheme 2. Synthesis of (*E*)-Norendoxifen (*E*-4)

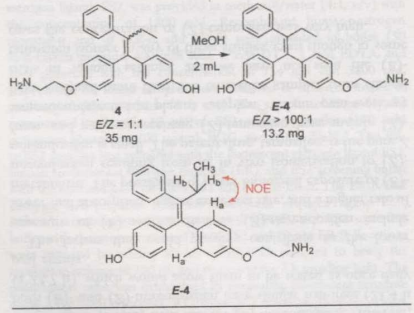

ifen was confirmed by NOE NMR spectroscopy. Irradiation of the H_a aromatic protons (Scheme 2) produced a clear NOE with the H_b benzylic methylene protons.

To prepare (*Z*)-norendoxifen, Gauthier et al.'s procedure[22] was used to stereospecifically synthesize the monopivalate **6** (Scheme 3). The McMurry coupling reaction of **5**[22] with propiophenone provided the crude product of **6** as a mixture with *E*:*Z* ratio 10:1. Trituration of the crude product with methanol gave **6** as the pure *E* isomer (*E*:*Z* > 100) in 69% yield. In the subsequent alkylation reaction, the isomerization of **6** occurred. By minimizing the amount of reaction solvent and use of 2-iodoacetamide in excess, the crude product **7** was obtained with *E*:*Z* ratio 13:1. Further purification by trituration with methanol improved *E*:*Z* to 25:1 with 67% yield. In the last step, the reduction of the amide and removal of the pivaloyl group were accomplished in one pot. Unfortunately, partial isomerization occurred, and (*Z*)-norendoxifen (**Z-4**) was obtained with an *E*:*Z* ratio of 1:10. Further trituration of the product with many different solvents (including methanol,

dx.doi.org/10.1021/jm400364h | J. Med. Chem. 2013, 56, 4611−4618

Scheme 3. Synthesis of (Z)-Norendoxifen (Z-4)[a]

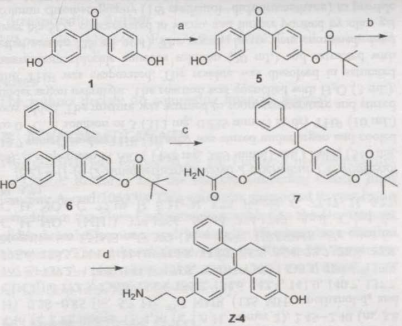

[a]Reagents and conditions: (a) NaH, *t*-BuCOCl, THF, 36%; (b) propiophenone, Zn, $TiCl_4$, THF, 69%; (c) ICH_2CONH_2, acetone, K_2CO_3, 67%; (d) LAH, $AlCl_3$, THF, 70%.

ethanol, hexanol, ethyl acetate, propanol, THF, and 2-propanol) did not improve the *E*:*Z* ratio.

The stabilities of (*E*)- and (*Z*)-norendoxifen in different solvents were also tested. Interestingly, if chloroform (or dichloromethane) was used as the single solvent, both (*E*)- and (*Z*)-norendoxifen underwent a fast isomerization to the mixed (*E*,*Z*)-norendoxifen. However, if methanol or methanol–chloroform mixture (v/v 1:1, good solubility for *E*-norendoxifen) was used as solvent, the isomerization rate was significantly decreased and the sample could be stored for at least a few weeks without substantial isomerization. This observation is similar to the isomerization of (*E*,*Z*)-4-hydroxytamoxifen reported by Yu et al.[19] The detailed mechanism of isomerization is still not fully understood.[23,24]

Biological Activity Evaluation. All of the compounds were tested for inhibition of aromatase activity and estrogen receptor binding affinities (including both ER-α and ER-β, Table 1). The IC_{50} value against aromatase for the mixed (*E*,*Z*)-norendoxifen (**4**) is 102 nM, which is quite close to the value (IC_{50} 90 nM) previously reported.[17] As expected, the mixed (*E*,*Z*)-norendoxifen also showed good binding affinities toward both ER-α and ER-β, with EC_{50} values in the nanomolar range (26.9 and 35.2 nM, respectively). The (*E*)-norendoxifen (***E*-4**) is about 10-fold more potent than the (*Z*)-norendoxifen (**Z-4**) when tested against aromatase (IC_{50} 77 vs 1029 nM). Because (*Z*)-norendoxifen (*E*:*Z* ratio 1:10) still contains a certain amount of (*E*)-norendoxifen (9%), the actual aromatase inhibitory activity for (*Z*)-norendoxifen is even weaker. For ER binding affinity, (*Z*)-norendoxifen is about 3-fold more potent than (*E*)-norendoxifen when tested against ER-α and ER-β, which is similar to the observation with 4-hydroxytamoxifen.[25] The aromatase inhibitory activity of diphenol **2** (IC_{50} 25 μM) is significantly weaker than the mixed (*E*,*Z*)-norendoxifen. Interestingly, the amide **3** (IC_{50} 9.3 μM) is also 90-fold less potent than the mixed (*E*,*Z*)-norendoxifen, indicating the importance of the aminoethoxy side chain for aromatase inhibition.

It was previously reported that commercial samples of (*E*,*Z*)-norendoxifen and (*E*)-norendoxifen had the same IC_{50} values

Table 1. The Aromatase Inhibitory Activity and Estrogen Receptor Binding Affinities of Norendoxifen and Structurally Related Compounds[a,b,c,d]

compd	aromatase (IC_{50}, nM, or percent inhibition)	aromatase (K_i, nM)	ER-α (EC_{50}, nM, or percent competition)	ER-β (EC_{50}, nM or percent competition)
(*E*,*Z*)-4	102.2 ± 32.7	77 ± 9.5	26.9 ± 4.8	35.2 ± 16.8
E-4	76.8 ± 33.3	48 ± 0.4	58.7 ± 1.0	78.5 ± 57.3
Z-4	1029 ± 318	442 ± 8	17.0 ± 1.9	27.5 ± 14.3
2	24880 ± 1360	ND	80% competition	306.9 + 106.4
3	9257 ± 195	ND	57% competition	71% competition
6	8% inhibition	ND	68% competition	68% competition
7	0% inhibition	ND	56% competition	45% competition

[a]ND = not determined. [b]The values are mean values of at least three experiments. [c]Percent aromatase inhibition was determined at the concentration of 50 μM for each compound. [d]Percent estrogen receptor competition was determined at the concentration of 100 μM for each compound.

(90 nM) vs aromatase,[17] while in the present case the IC_{50} values of (*E*,*Z*)-norendoxifen (102 nM) and (*E*)-norendoxifen (77 nM) are different. During the course of the present studies, an appreciation was gained for how readily isomerization can occur and precautions were implemented to prevent it.

Molecular Modeling. A molecular docking study was performed to investigate the norendoxifen–aromatase interaction and provide a basis for further structure-based drug design. (*E*)-Norendoxifen (***E*-4**) was docked into the aromatase androgen binding site (PDB 3s79) using GOLD 3.0 software, and the resulting structure was fully energy minimized using the Amber 10 molecular dynamics package. The hypothetical binding mode of (*E*)-norendoxifen in the active site of aromatase is shown in Figure 2. The phenolic hydroxyl group forms a hydrogen bond with the backbone carbonyl group of Leu372. The ether oxygen hydrogen bonds to the side chain hydroxyl group of Ser478. According to the testing results, the terminal amino group is crucial for aromatase inhibitory activity because the amide **3** is much less active than norendoxifen. Here, the amino group displayed a dual interaction with the carbonyl group (hydrogen bond) and carboxyl group (salt bridge) of Asp309. The dual interaction also explains the previous testing results that replacing the amino group with a methylamino group (endoxifen, IC_{50} 6 μM) or dimethylamino group (4-hydroxytamoxifen, IC_{50} 530 μM) significantly reduced the aromatase inhibitory activity.[17] Besides the polar interactions, the unsubstituted phenyl ring and the ethyl group point toward the heme and are surrounded by hydrophobic residues Ile133 and Val370. Because this model is consistent with the aromatase inhibitory testing results for our compounds and the previously reported tamoxifen metabolites, it can provide a rational basis for further structure-based drug design.

The docking pose displayed in Figure 2 is revised relative to a previously proposed structure.[17] The new pose resulted from the use of the recently released aromatase crystal structure (PDB ID 3s79), which has slightly higher resolution than the structure used before (PDB ID 3s79 3eqm). A more significant difference is that in the present case, all crystal water molecules were removed before docking, thus making space for the aminoethoxy side chain of the ligand. According to what I saw

dx.doi.org/10.1021/jm200281n | J. Med. Chem. 2011, 54, 4611–4618

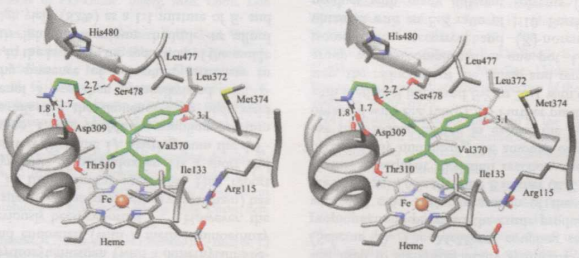

Figure 2. The hypothetical binding mode of (*E*)-norendoxifen (*E*-4, green) in the active site of human aromatase. The stereoview is programmed for wall-eyed (relaxed) viewing.

calculations, the docking pose displayed in Figure 2 has a lower calculated binding energy (ΔG = −46.11 kcal/mol) than the previous structure (ΔG = −38.80 kcal/mol). As stated above, this pose also has the advantage of offering an explanation for the observed decrease in aromatase inhibitory activity when the primary amino group is changed to a methylamino group or a dimethylamino group.[17]

Pharmacokinetics. To explore the pharmacokinetic profile and oral bioavailability for (*E*)- and (*Z*)-norendoxifen, (*E,Z*)-norendoxifen (**4**) was administered to NOD/SCID female mice. Plasma concentrations of (*E*)- and (*Z*)-norendoxifen were determined after a single oral dose of 100 mg/kg (Figure 3), and the pharmacokinetic parameters for both (*E*)- and (*Z*)-norendoxifen were calculated (Table 2). The results reveal that (*Z*)-norendoxifen has a more rapid absorption than (*E*)-norendoxifen (T_{max} 1 h vs 2 h), and its peak plasma concentration is 3-fold higher than that of (*E*)-norendoxifen.

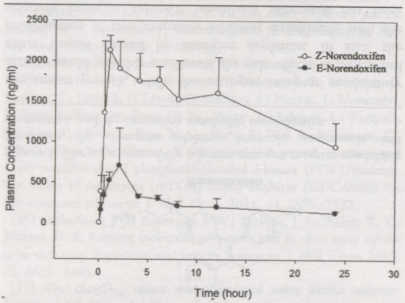

Figure 3. Time-dependent plasma concentration of (*E*)- and (*Z*)-norendoxifen following a single oral dose of the mixed (*E,Z*)-norendoxifen (100 mg/kg).

The area under the curve (AUC) for (*Z*)-norendoxifen is also much higher (6-fold) than that for (*E*)-norendoxifen. However, both (*E*)- and (*Z*)-norendoxifen have similar half-lives (21.4 h vs 22.7 h), which would allow them to be tested as once daily oral agents.

The factors that could possibly contribute to the lower exposure of (*E*)-norendoxifen vs (*Z*)-norendoxifen include lower oral absorption, higher excretion rate, and a higher rate of metabolism. The possibility of lower biological exposure of (*E*)-norendoxifen resulting from its in vivo isomerization to (*Z*)-norendoxifen is small. The parent drug, tamoxifen, is the pure *Z* form, and patients receiving (*Z*)-tamoxifen have mainly (*Z*)-tamoxifen detected in plasma samples.[26] In our own work we have analyzed more than 500 tamoxifen samples from clinical trials in various settings, and we have not seen the (*E*)-tamoxifen isomer in any of these studies, even though in some cases the concentration of (*Z*)-tamoxifen was very high.

■ CONCLUSION

Mixed (*E,Z*)-, (*E*)-, and (*Z*)-norendoxifen have been prepared via a short and convenient synthetic approach. The mixed (*E,Z*)-norendoxifen exhibits potent aromatase inhibitory activity (IC_{50} 102 nM) while also displaying good binding affinity to both ER-α (EC_{50} 27 nM) and ER-β (EC_{50} 35 nM). (*E*)-Norendoxifen is the active component for aromatase inhibition because it is at least 10 times more active than (*Z*)-norendoxifen. In contrast, the (*Z*)-norendoxifen has slightly better binding affinity toward ER-α and ER-β than the (*E*)-norendoxifen. The possible binding mode of (*E*)-norendoxifen with aromatase was investigated by molecular modeling techniques, providing a result that can serve as the basis for further structure-based drug design. It is possible that (*E*)-norendoxifen or a closely related analogue could be an effective aromatase inhibitor with fewer side effects than aromatase inhibitors currently in use because of estrogenic effects in noncancerous cells in muscular and skeletal tissues.

Table 2. Pharmacokinetic Parameters for (E)- and (Z)-Norendoxifen in Mice[a]

compd	T_{max} (h)	C_{max} (μg/mL)	C_{last} (μg/mL)	$T_{1/2}$ (h)	AUC_{last} (h·μg/L)	Vz_F_obs (L)	Cl_F_obs (L/h)
(*E*)-norendoxifen	2	0.7	0.1	21.4	5.8	2.8	0.091
(*Z*)-norendoxifen	1	2.1	0.9	22.7	35.1	0.5	0.016

[a]The data are mean concentrations in mouse plasma (n = 3) following a single oral dose of the mixed (*E,Z*)-norendoxifen (100 mg/kg).

dx.doi.org/10.1021/jm400364h | J. Med. Chem. 2013, 56, 4611−4618

EXPERIMENTAL SECTION

General. Melting points were determined using capillary tubes with a Mel-Temp apparatus and are uncorrected. The nuclear magnetic resonance (^{1}H and ^{13}C NMR) spectra were recorded using a Bruker ARX300 spectrometer (300 MHz) with a QNP probe or a Bruker DRX-2 spectrometer (500 MHz) with a BBO probe. High-resolution mass spectra were recorded on a double-focusing sector mass spectrometer with magnetic and electrostatic mass analyzers. The purities of biologically important compounds are ≥95% as determined by elemental analyses, with the observed percentages differing less that 0.40% from the calculated values. Cytochrome P450 (CYP) inhibitor screening kit for aromatase (CYP19) was purchased from BD Biosciences (San Jose, CA). Estrogen receptor α and β competitor assay kits were purchased from Invitrogen (Carlsbad, CA).

4,4′-(2-Phenylbut-1-ene-1,1-diyl)diphenol (2).[19] Zinc powder (10.11 g, 154 mmol) was suspended in dry THF (100 mL), and the mixture was cooled to 0 °C. $TiCl_4$ (7.5 mL, 70 mmol) was added dropwise under argon. When the addition was complete, the mixture was warmed to room temperature and heated to reflux for 2 h. After cooling down, a solution of 4,4′-dihydroxybenzophenone (2.63 g, 12.3 mmol) and propiophenone (5.15 g, 38.4 mmol) in dry THF (100 mL) was added at 0 °C and the mixture was heated at reflux in the dark for 2.5 h. After being cooled to room temperature, the zinc dust was filtered off and THF was evaporated. The residue was dissolved with saturated ammonium chloride aqueous solution (150 mL) and extracted with ethyl acetate (120 mL × 6). The organic layers were combined and dried over Na_2SO_4, concentrated in vacuo, and further purified by silica gel column chromatography (2:1 hexanes−ethyl acetate) to provide the product **2** as yellow solid (3.4 g, 88%): mp 200−202 °C (lit.[19] 200.6 °C). ^{1}H NMR (300 MHz, acetone-d_6) δ 7.16−7.04 (m, 7 H), 6.84−6.81 (m, 2 H), 6.70−6.67 (m, 2 H), 6.48−6.45 (m, 2 H), 2.47 (q, J = 7.5 Hz, 2 H), 0.88 (t, J = 7.5 Hz, 3 H). Anal. Calcd for $C_{22}H_{20}O_2$: C, 83.51; H, 6.37. Found: C, 83.21; H, 6.31.

(E,Z)-2-(4-(1-(4-Hydroxyphenyl)-2-phenylbut-1-enyl)phenoxy)-acetamide (3). A suspension of **2** (3.4 g, 10.7 mmol) and K_2CO_3 (4.22 g, 30.5 mmol) in acetone (60 mL) was heated to reflux for 10 min. A solution of 2-iodoacetamide (2.4 g, 13 mmol) in acetone (20 mL) was added in small portions over 3 h, and the mixture was stirred for 1 h. After cooling down, acetone was evaporated and the residue was dissolved in saturated ammonium chloride aqueous solution (120 mL) and extracted with ethyl acetate (120 mL × 5). The organic layers were combined, dried over Na_2SO_4, concentrated in vacuo, and further purified by silica gel column chromatography (1:2 hexanes−ethyl acetate) to provide the product **3** as white solid (1.8 g, 45%) as a 5:4 mixture of E and Z isomers: mp 193−196 °C. ^{1}H NMR (500 MHz, methanol-d_4 and $CDCl_3$) δ 7.14−6.98 (m, 13 H), 6.91−6.89 (m, 2 H, isomer 1), 6.76−6.73 (m, 3.2 H, isomer 2), 6.63−6.61 (m, 2 H, isomer 1), 6.55−6.53 (m, 1.6 H, isomer 2), 6.40−6.38 (m, 2 H, isomer 1), 4.46 (s, 2 H, isomer 1), 4.30 (s, 1.6 H, isomer 2), 2.45−2.40 (m, 3.8 H), 0.88−0.85 (m, 5.7 H). ^{13}C NMR (125 MHz, methanol-d_4 and $CDCl_3$) δ 172.5, 156.0, 155.5, 155.2, 154.6, 142.4, 141.0, 140.7, 137.7, 137.5, 137.2, 134.8, 134.4, 131.8, 131.7, 130.5, 130.3, 129.4, 127.5, 125.6, 125.5, 114.6, 114.0, 113.8, 113.2, 66.6, 66.4, 28.7, 28.6, 12.9. Negative ion ESIMS m/z 372 ($M - H^+$)$^-$. HRESIMS m/z calcd for $C_{24}H_{24}NO_3^-$ (MH^+) 374.1756, found 374.1749. Anal. Calcd for $C_{24}H_{23}NO_3$: C, 77.19; H, 6.21; N, 3.75. Found: C, 77.17; H, 6.27; N, 3.72.

(E,Z)-4-(1-(4-(2-Aminoethoxy)phenyl)-2-phenylbut-1-enyl)phenol (4). A suspension of $AlCl_3$ (492 mg, 3.69 mmol) and $LiAlH_4$ (510 mg, 12.7 mmol) in dry THF (10 mL) was stirred under argon and cooled to 0 °C. A solution of **3** (312 mg, 0.835 mmol) in dry THF (10 mL) was added. The mixture was warmed to room temperature and stirred under argon overnight. The reaction was quenched with H_2O (3 mL), and THF was evaporated. The residue was dissolved in saturated ammonium chloride aqueous solution (20 mL) and extracted with ethyl acetate (25 mL × 4). The organic layers were combined, dried over Na_2SO_4, concentrated in vacuo, and further purified by silica gel column chromatography (1:9 methanol−dichloromethane) to provide the product **4** as a white solid (245 mg, 82%) consisting of a 5:4 mixture of E and Z isomers: mp 204−209 °C. ^{1}H NMR (500 MHz, $CDCl_3$ and methanol-d_4) δ 7.10−6.99 (m, 13 H), 6.84−6.82 (m, 2 H, E isomer), 6.75−6.71 (m, 3.4 H, Z isomer), 6.63−6.61 (m, 2 H, E isomer), 6.49−6.47 (m, 1.6 H, Z isomer), 6.40−6.39 (m, 2 H, E isomer), 3.99 (t, J = 5.1 Hz, 2 H, E isomer), 3.83 (t, J = 5.1 Hz, 1.6 H, Z isomer), 3.02 (t, J = 5.1 Hz, 2 H, E isomer), 2.92 (t, J = 5.1 Hz, 1.6 H, Z isomer), 2.45−2.39 (m, 3.6 H), 0.87−0.84 (m, 5.5 H). ^{13}C NMR (125 MHz, $CDCl_3$ and methanol-d_4) δ 157.1, 156.2, 155.3, 154.4, 142.6, 142.5, 140.7, 140.5, 137.8, 136.7, 136.3, 135.0, 134.6, 131.8, 130.5, 130.4, 129.5, 127.5, 125.6, 114.6, 113.9, 113.8, 113.0, 68.5, 68.2, 40.5, 40.4, 28.7, 13.2. ESIMS m/z 360 (MH^+). HRESIMS m/z calcd for $C_{24}H_{26}NO_2^+$ (MH^+) 360.1964, found 360.1959. Anal. Calcd for $C_{24}H_{25}NO_2$: C, 80.19; H, 7.01; N, 3.90. Found: C, 79.98; H, 7.15; N, 3.98.

(E)-4-(1-(4-(2-Aminoethoxy)phenyl)-2-phenylbut-1-enyl)phenol (E-4). Trituration of norendoxifen (**4**, 35 mg, E:Z = 5:4) with methanol (2 mL) gave pure (*E*)-norendoxifen (*E*-**4**, E:Z > 100:1) as a white solid (13.2 mg, 38%): mp 206−208 °C. ^{1}H NMR (300 MHz, $CDCl_3$ and methanol-d_4) δ 7.13−7.03 (m, 7 H), 6.88−6.85 (m, 2 H), 6.65−6.61 (m, 2 H), 6.42−6.39 (m, 2 H), 4.00 (t, J = 5.1 Hz, 2 H), 3.02 (t, J = 5.1 Hz, 2 H), 2.43 (q, J = 7.4 Hz, 2 H), 0.88 (t, J = 7.4 Hz, 3 H). ^{13}C NMR (125 MHz, $CDCl_3$ and methanol-d_4) δ 157.2, 154.4, 142.5, 140.5, 137.8, 136.6, 134.6, 131.8, 130.4, 129.5, 127.5, 125.6, 113.9, 113.7, 69.0, 40.7, 28.7, 13.2. ESIMS m/z 360 (MH^+). HRESIMS m/z calcd for $C_{24}H_{26}NO_2^+$ (MH^+) 360.1964, found 360.1964. Anal. Calcd for $C_{24}H_{25}NO_2$·0.15$CHCl_3$: C, 76.86; H, 6.72; N, 3.71. Found: C, 76.75; H, 6.99; N, 3.49.

(E)-4-(1-(4-Hydroxyphenyl)-2-phenylbut-1-enyl)phenyl Pivalate (6).[22] Zinc powder (446 mg, 6.82 mmol) was suspended in dry THF (8 mL), and the mixture was cooled to 0 °C. $TiCl_4$ (0.4 mL, 3.7 mmol) was added dropwise under argon. When the addition was complete, the mixture was warmed to room temperature and heated to reflux for 2 h. After cooling down, a solution of 4-(4-hydroxybenzoyl)-phenyl pivalate (**5**, 257 mg, 0.861 mmol) and propiophenone (374 mg, 2.79 mmol) in dry THF (10 mL) was added, and the mixture was heated at reflux in the dark for 2.5 h. After being cooled to room temperature, the zinc dust was filtered off and THF was carefully evaporated. The residue was dissolved in saturated ammonium chloride aqueous solution (30 mL) and extracted with ethyl acetate (40 mL × 4). The organic layers were combined, dried over Na_2SO_4, concentrated in vacuo, and further purified by silica gel column chromatography (4:1 hexanes−ethyl acetate) to afford the product **6** as white solid (323 mg, 94%). The NMR spectrum showed an E:Z ratio of 10:1. Trituration with methanol (2 mL) provided the pure E isomer (E:Z > 100:1) as white solid (238 mg, 69%): mp 162−164 °C (lit.[22] 165−167 °C). ^{1}H NMR (300 MHz, methanol-d_4) δ 7.25−7.22 (m, 2 H), 7.16−7.08 (m, 5 H), 7.05−7.02 (m, 2 H), 6.68−6.64 (m, 2 H), 6.42−6.39 (m, 2 H), 2.46 (q, J = 7.4 Hz, 2 H), 1.36 (s, 9 H), 0.91 (t, J = 7.4 Hz, 3 H). Anal. Calcd for $C_{27}H_{28}O_3$·0.8MeOH: C, 78.35; H, 7.38. Found: C, 78.26; H, 6.99.

(E)-4-(1-(4-(2-Amino-2-oxoethoxy)phenyl)-2-phenylbut-1-enyl)-phenyl Pivalate (7). A mixture of **6** (226 mg, 0.565 mmol), 2-iodoacetamide (434 mg, 2.35 mmol), and K_2CO_3 (440 mg, 3.18 mmol) was dissolved in acetone (8 mL). The suspension was heated to reflux and stirred for 2 h. After cooling down, acetone was carefully evaporated and the residue was dissolved in saturated ammonium chloride aqueous solution (20 mL) and extracted with ethyl acetate (20 mL × 3). The organic layers were combined, dried over Na_2SO_4, concentrated in vacuo, and further purified by silica gel column chromatography (1:1 hexanes−ethyl acetate) to provide the product **7** as a white solid (203 mg, 78.5%). The NMR spectrum shows an E:Z ratio of 13:1. Trituration with methanol (3 mL) provided the pure E isomer (E:Z > 25:1) as a white solid (174 mg, 67%): mp 167−169 °C. ^{1}H NMR (300 MHz, $CDCl_3$) δ 7.26−7.20 (m, 2 H), 7.18−7.04 (m, 7 H), 6.82−6.79 (m, 2 H), 6.57−6.54 (m, 2 H), 4.35 (s, 2 H), 2.47 (q, J = 7.4 Hz, 2 H), 1.37 (s, 9 H), 0.92 (t, J = 7.4 Hz, 3 H). ^{13}C NMR (75 MHz, $CDCl_3$) δ 177.1, 171.2, 155.0, 149.7, 142.3, 142.0, 140.8, 137.0, 136.8, 132.2, 130.4, 129.6, 127.9, 126.2, 121.2, 113.5, 66.9, 39.1, 29.0, 27.1, 13.5. ESIMS m/z 480 (MNa^+). HRESIMS m/z calcd for $C_{29}H_{31}NO_4Na$ (MNa^+) 480.2151, found 480.2148. Anal. Calcd for

dx.doi.org/10.1021/jm400364h | J. Med. Chem. 2013, 56, 4611−4618

$C_{29}H_{31}NO_4$: C, 76.12; H, 6.83; N, 3.06. Found: C, 75.88; H, 6.88; N, 3.06.

(Z)-4-(1-(4-(2-Aminoethoxy)phenyl)-2-phenylbut-1-enyl)phenol (Z-4). A suspension of $AlCl_3$ (135 mg, 1.01 mmol) and $LiAlH_4$ (195 mg, 5.14 mmol) in dry THF (5 mL) was stirred under argon and the mixture was cooled to 0 °C. A solution of 7 (95.1 mg, 0.208 mmol, *E*:*Z* > 25:1) in dry THF (5 mL) was added. The mixture was warmed to room temperature and stirred under argon for 3 h. The reaction was quenched with H_2O (0.5 mL), and THF was evaporated. The residue was dissolved in saturated ammonium chloride aqueous solution (20 mL) and extracted with ethyl acetate (20 mL × 5). The organic layers were combined, dried over Na_2SO_4, concentrated in vacuo, and further purified by silica gel column chromatography (1:9 methanol–dichloromethane) to provide the product **Z-4** as white solid (52 mg, 70%): mp 176–179 °C. The NMR spectrum indicated an *E*:*Z* ratio of 1:10. ^{1}H NMR (300 MHz, methanol-d_4) δ 7.15–7.05 (m, 5.6 H), 7.03–6.98 (m, 2.2 H), 6.95–6.92 (m, 0.20 H, *E* isomer), 6.76–6.72 (m, 4 H, *Z* isomer), 6.66–6.63 (m, 0.20 H, *E* isomer), 6.58–6.54 (m, 2 H, *Z* isomer), 6.41–6.38 (m, 0.20 H, *E* isomer), 4.04 (t, J = 5.3 Hz, 0.20 H, *E* isomer), 3.86 (t, J = 5.3 Hz, 2 H, *Z* isomer), 3.03 (t, J = 5.3 Hz, 0.20 H, *E* isomer), 2.92 (t, J = 5.3 Hz, 2 H, *Z* isomer), 2.48 (q, J = 7.3 Hz, 2.2 H), 0.90 (t, J = 7.3 Hz, 3.4 H). ESIMS m/z 360 (MH^+). HRESIMS m/z calcd for $C_{24}H_{26}NO_2$ (MH^+) 360.1964, found 360.1965. Anal. Calcd for $C_{24}H_{25}NO_2$: C, 80.19; H, 7.01; N, 3.90. Found: C, 79.99; H, 7.08; N, 3.87.

Molecular Modeling. The structure of (*E*)-norendoxifen was constructed with Sybyl 7.1 software and energy minimized to a gradient of 0.01 kcal/mol by the Powell method using Gasteiger–Huckel charges and the Tripos force field. The crystal structure of aromatase was obtained from the Protein Data Bank (ID: 3s79), and the natural ligand (androstenedione) and all crystal water molecules were removed. The (*E*)-norendoxifen was docked into the androstenedione binding pocket in aromatase using the GOLD 3.0 program. The top five docking solutions according to the GOLD fitness score were selected, and the corresponding ligand–protein complexes were thoroughly energy minimized by the Amber 10 molecular dynamics package. The Amber parm99 force field was used for the protein during energy minimization. For the ligand, the force field parameters were taken from the General Amber Force Field (GAFF), whereas the atomic partial charges were derived from the AM1-BCC method implemented by antechamber. The ligand–protein binding energy for each energy-minimized complex was calculated using the MM-PBSA method. The complex with the lowest binding energy was selected out as the best binding pose for (*E*)-norendoxifen.

Inhibition of Recombinant Human Aromatase (CYP19) by Microsomal Incubations. The activity of recombinant aromatase (CYP19) was determined by measuring the conversion rate of fluorometric substrate 7-methoxy-4-trifluoromethylcoumarin (MFC) to its fluorescent metabolite 7-hydroxytrifluoromethylcoumarin (HFC). Experimental procedures were consistent with the published methodology.[27] All the incubations were performed using incubation times and protein concentrations that were within the linear range for reaction velocity. The fluorometric substrate, MFC, was dissolved in acetonitrile with the final concentration of 25 mM. All tested samples were dissolved in either methanol or methanol/dichloromethane (1:1, v/v). The sample solutions (2 μL) were mixed well with 98 μL of NADPH-Cofactor Mix (16.25 μM $NADP^+$, 825.14 μM $MgCl_2$, 825.14 μM glucose-6-phosphate, and 0.4 units/mL glucose-6-phosphate dehydrogenase) and were prewarmed for 10 min at 37 °C. Enzyme/substrate mix was prepared with fluorometric substrate, recombinant human aromatase (CYP19), and 0.1 M potassium phosphate buffer (pH 7.4). Reactions were initiated by adding 100 μL of enzyme/substrate mix to bring the incubation volume to 200 μL and incubated for 30 min. All the reactions were stopped by adding 75 μL of 0.1 M Tris base dissolved in acetonitrile. The amount of fluorescent product was determined immediately by measuring fluorescent response using a BioTek (Winooski, VT) Synergy 2 fluorometric plate reader. Excitation–emission wavelengths for MFC metabolite were 409–530 nm. The standard curve for MFC metabolite was constructed using the appropriate fluorescent metabolite standards. Quantification of samples was performed by applying the linear regression equation of the standard curve to the fluorescence response. The limit of quantification for the metabolites of MFC was 24.7 pmol with intra- and interassay coefficients of variation less than 10%.

Kinetic Analysis of Recombinant Human Aromatase (CYP19). The rates of metabolite formation in the presence of the test inhibitors were compared with those in the control, in which the inhibitor was replaced with vehicle. The extent of enzyme inhibition was expressed as percentage of remaining enzyme activity compared to the control. IC_{50} values were determined as the inhibitor concentrations which brought about half reduction in enzyme activity by fitting all the data to a one-site competition equation using Graphpad Prism 5.0 (GraphPad Software Inc., San Diego, CA). To characterize the inhibitory mechanism of norendoxifen against aromatase (CYP19), all inhibitory data by norendoxifen at different substrate concentrations were plotted as Lineweaver–Burk plots. The inhibitory constant K_i values were determined by nonlinear least-squares regression analysis using Graphpad Prism 5.0 (GraphPad Software Inc., San Diego, CA). Before modeling the data using nonlinear models, initial information about the inhibitory mechanism was obtained by visual inspection of Lineweaver–Burk plots. Final decision on the mechanism of inhibition was made on model-derived parameters such as R^2 (or R Square) and absolute sum of squares.

Binding Affinities for Recombinant Human Estrogen Receptor α and β (ER-α and ER-β). The binding affinities for estrogen receptor-α and -β were determined by measuring the change of polarization value when the fluorescent estrogen ligand, ES2, was displaced by the tested compounds. Experimental procedures were consistent with the protocol provided by Invitrogen. The fluorescent estrogen ligand, ES2, was provided in methanol/water (4:1, v/v) with the concentration of 1800 nM. Recombinant human estrogen receptor-α and -β (ER-α and ER-β) were provided in buffer (50 mM bis-tris propane, 400 mM KCl, 2 mM DTT, 1 mM EDTA, and 10% glycerol), with the concentration of 734 nM and 3800 nM, respectively. All tested samples were dissolved in either methanol or methanol/dichloromethane (1:1, v/v). The sample solutions (1 μL) were mixed well with 49 μL of ES2 screening buffer (100 mM potassium phosphate, 100 μg/mL BGG, and 0.02% NaN_3). The ER-α/ES2 complex was prepared with the fluorescent estrogen ligand ES2, human recombinant estrogen receptor (ER), and ES2 screening buffer with the concentration of 9 nM ES2 and 30 nM ER-α. The ER-β/ES2 complex was prepared with the fluorescent estrogen ligand ES2, human recombinant estrogen receptor-β (ER-β), and ES2 screening buffer with the concentration of 9 nM ES2 and 20 nM ER-β. Reactions were initiated by adding 50 μL of ER/ES2 complex to bring the incubation volume to 100 μL and incubated for 2 h avoiding light. The polarization value was determined by measuring fluorescent response using a BioTek (Winooski, VT) Synergy 2 fluorometric plate reader. Excitation–emission wavelengths for fluorescence polarization were 485–530 nm. The polarization value in the presence of the test competitors were compared with those in control in which the competitor was replaced with vehicle. The extent of competition was expressed as percentage of remaining polarization compared to the control. EC_{50} values were determined as the competitor concentrations which brought about half reduction in polarization value by fitting all the data to a one-site competition equation using Graphpad Prism 5.0 (GraphPad Software Inc., San Diego, CA).

Pharmacokinetics. The mixed (*E*,*Z*)-norendoxifen (100 mg/kg, *E*:*Z* of 45:55 determined by LC-MS-MS analysis) was given to 10-week-old NOD/SCID female mice (The Jackson Laboratory, Bar Harbor, Maine) by oral gavages according to local IUCUC approved animal protocol. Each mouse was bled for only one time point. Blood samples were collected by tail vein bleeding (n = 3 for each time point) at different time points up to 24 h. Plasma levels of both (*E*)- and (*Z*)-norendoxifen were analyzed by LC-MS-MS method and plotted against time. The relative concentrations of *E* and *Z* isoforms are determined by their AUC in LC-MS-MS analysis. The identity of each peak was confirmed by purified *E* and *Z* isomers. Pharmacokinetic parameters were further obtained by noncompartmental modeling (Winnonlin 6.2).

AUTHOR INFORMATION

Corresponding Author

*Phone: 765-494-1465. Fax: 765-494-6790. E-mail: cushman@purdue.edu.

Notes

The authors declare no competing financial interest.

ACKNOWLEDGMENTS

This research was supported by the Purdue University Center for Cancer Research and the Indiana University Center Joint Funding Award 206330. This work was supported in part by an award from the Floss Endowment, provided to the Department of Medicinal Chemistry and Molecular Pharmacology, Purdue University. The authors acknowledge Dr. Richard F. Bergstrom for advice on pharmacokinetic analysis, and Dr. Huaping Mo for his help with NMR spectroscopy.

ABBREVIATIONS USED

AIs, aromatase inhibitors; AUC, area under the curve; ER, estrogen receptor; LAH, lithium aluminum hydride; PDB, Protein Data Bank

REFERENCES

(1) *Cancer Facts & Figures 2012*; American Cancer Society: Atlanta, 2012.

(2) Jordan, V. C.; Brodie, A. M. H. Development and Evolution of Therapies Targeted to the Estrogen Receptor for the Treatment and Prevention of Breast Cancer. *Steroids* **2007**, *72*, 7–25.

(3) Davies, C.; Godwin, J.; Gray, R.; Clarke, M.; Darby, S.; McGale, P.; Wang, Y. C.; Peto, R.; Godwin, J.; Pan, H. C.; Cutter, D.; Taylor, C.; Ingle, J. Early Breast Cancer Trialists' Collaborative Group (EBCTCG). Relevance of Breast Cancer Hormone Receptors and Other Factors to the Efficacy of Adjuvant Tamoxifen: Patient-Level Meta-Analysis of Randomised Trials. *Lancet* **2011**, *378*, 771–784.

(4) Riggs, B. L.; Hartmann, L. C. Drug Therapy: Selective Estrogen-Receptor Modulators—Mechanisms of Action and Application to Clinical Practice. *N. Engl. J. Med.* **2003**, *348*, 618–629.

(5) Ali, S.; Coombes, R. C. Endocrine-Responsive Breast Cancer and Strategies for Combating Resistance. *Nature Rev. Cancer* **2002**, *2*, 101–112.

(6) Davies, C.; Pan, H. C.; Godwin, J.; Gray, R.; Arriagada, R.; Raina, V.; Abraham, M.; Alencar, V. H. M.; Badran, A.; Bonfill, X.; Bradbury, J.; Clarke, M.; Collins, R.; Davis, S. R.; Delmestri, A.; Forbes, J. F.; Haddad, P.; Hou, M. F.; Inbar, M.; Khaled, H.; Kielanowska, J.; Kwan, W. H.; Mathew, B. S.; Mittra, I.; Muller, B.; Nicolucci, A.; Peralta, O.; Pernas, F.; Petruzelka, L.; Pienkowski, T.; Radhika, R.; Rajan, B.; Rubach, M. T.; Tort, S.; Urrutia, G.; Valentini, M.; Wang, Y. C.; Peto, R. Long-Term Effects of Continuing Adjuvant Tamoxifen to 10 Years Versus Stopping at 5 Years after Diagnosis of Oestrogen Receptor-Positive Breast Cancer: ATLAS, a Randomised Trial. *Lancet* **2013**, *381*, 805–816.

(7) Bonneterre, J.; Buzdar, A.; Nabholtz, J. M. A.; Robertson, J. F. R.; Thurlimann, B.; von Euler, M.; Sahmoud, T.; Webster, A.; Steinberg, M.; Arimidex Writing, C.; Investigators Comm, M. Anastrozole Is Superior to Tamoxifen as First-Line Therapy in Hormone Receptor Positive Advanced Breast Carcinoma—Results of Two Randomized Trials Designed for Combined Analysis. *Cancer* **2001**, *92*, 2247–2258.

(8) Mouridsen, H.; Gershanovick, M.; Sun, Y.; Perez-Carrion, R.; Boni, C.; Monnier, A.; Apffelstaedt, J.; Smith, R.; Sleeboom, H. P.; Jaenicke, F.; Pluzanska, A.; Dank, M.; Becquart, D.; Bapsy, P. P.; Salminen, E.; Snyder, R.; Chaudri-Ross, H.; Lang, R.; Wyld, P.; Bhatnagar, A. Phase III Study of Letrozole Versus Tamoxifen as First-Line Therapy of Advanced Breast Cancer in Postmenopausal Women: Analysis of Survival and Update of Efficacy from the International Letrozole Breast Cancer Group. *J. Clin. Oncol.* **2003**, *21*, 2101–2109.

(9) Nabholtz, J. M.; Bonneterre, J.; Buzdar, A.; Robertson, J. F. R.; Thurlimann, B.; Arimidex Writing Comm Behalf, I. Anastrozole (Arimidex (Tm)) versus Tamoxifen as First-Line Therapy for Advanced Breast Cancer in Postmenopausal Women: Survival Analysis and Updated Safety Results. *Eur. J. Cancer* **2003**, *39*, 1684–1689.

(10) Howell, A.; Cuzick, J.; Baum, M.; Buzdar, A.; Dowsett, M.; Forbes, J. F.; Hoctin-Boes, G.; Houghton, I.; Locker, G. Y.; Tobias, J. S.; Grp, A. T. Results of the ATAC (Arimidex, Tamoxifen, Alone or in Combination) Trial after Completion of 5 Years' Adjuvant Treatment for Breast Cancer. *Lancet* **2005**, *365*, 60–62.

(11) Thurlimann, B.; Keshaviah, A.; Coates, A. S.; Mouridsen, H.; Mauriac, L.; Forbes, J. F.; Paridaens, R.; Castiglione-Gertsch, M.; Gelber, R. D.; Rabaglio, M.; Smith, I.; Wardly, A.; Price, K. N.; Goldhirsch, A.; Grp, B. I. G. C. A Comparison of Letrozole and Tamoxifen in Postmenopausal Women with Early Breast Cancer. *N. Engl. J. Med.* **2005**, *353*, 2747–2757.

(12) Heshmati, H. M.; Khosla, S.; Robins, S. P.; O'Fallon, W. M.; Melton, L. J.; Riggs, B. L. Role of Low Levels of Endogenous Estrogen in Regulation of Bone Resorption in Late Postmenopausal Women. *J. Bone Miner. Res.* **2002**, *17*, 172–178.

(13) Ewer, M. S.; Gluck, S. A Woman's Heart the Impact of Adjuvant Endocrine Therapy on Cardiovascular Health. *Cancer* **2009**, *115*, 1813–1826.

(14) Bird, B.; Swain, S. M. Cardiac Toxicity in Breast Cancer Survivors: Review of Potential Cardiac Problems. *Clin. Cancer Res.* **2008**, *14*, 14–24.

(15) Bundred, N. J. The Effects of Aromatase Inhibitors on Lipids and Thrombosis. *Br. J. Cancer* **2005**, *93*, S23–S27.

(16) Khan, Q. J.; O'Dea, A. P.; Sharma, P. Musculoskeletal Adverse Events Asociated with Adjuvant Aromatase Inhibitors. *J. Oncol.* **2010**, 8.

(17) Lu, W. J.; Xu, C.; Pei, Z. F.; Mayhoub, A. S.; Cushman, M.; Flockhart, D. A. The Tamoxifen Metabolite Norendoxifen Is a Potent and Selective Inhibitor of Aromatase (Cyp19) and a Potential Lead Compound for Novel Therapeutic Agents. *Breast Cancer Res. Treat.* **2012**, *133*, 99–109.

(18) Baum, M.; Buzdar, A. U.; Cuzick, J.; Forbes, J.; Houghton, J.; Klijn, J. G. M.; Sahmoud, T.; Grp, A. T. Anastrozole Alone or in Combination with Tamoxifen Versus Tamoxifen Alone for Adjuvant Treatment of Postmenopausal Women with Early Breast Cancer: First Results of the ATAC Randomised Trial. *Lancet* **2002**, *359*, 2131–2139.

(19) Yu, D. D.; Forman, B. M. Simple and Efficient Production of (*Z*)-4-Hydroxytamoxifen, a Potent Estrogen Receptor Modulator. *J. Org. Chem.* **2003**, *68*, 9489–9491.

(20) Detsi, A.; Koufaki, M.; Calogeropoulou, T. Synthesis of (*Z*)-4-Hydroxytamoxifen and (*Z*)-2-4-1-(*P*-Hydroxyphenyl)-2-Phenyl-1-Butenyl Phenoxyacetic Acid. *J. Org. Chem.* **2002**, *67*, 4608–4611.

(21) Fauq, A. H.; Maharvi, G. M.; Sinha, D. A Convenient Synthesis of (*Z*)-4-Hydroxy-N-desmethyltamoxifen (Endoxifen). *Bioorg. Med. Chem. Lett.* **2010**, *20*, 3036–3038.

(22) Gauthier, S.; Mailhot, J.; Labrie, F. New Highly Stereoselective Synthesis of (*Z*)-4-Hydroxytamoxifen and (*Z*)-4-Hyrdoxytoremifene via McMurry Reaction. *J. Org. Chem.* **1996**, *61*, 3890–3893.

(23) Katzenellenbogen, J. A.; Carlson, K. E.; Katzenellenbogen, B. S. Facile Geometric Isomerization of Phenolic Non-Steroidal Estrogens and Antiestrogens: Limitations to the Interpretation of Experiments Characterizing the Activity of Individual Isomers. *J. Steroid Biochem. Mol. Biol.* **1985**, *22*, 589–596.

(24) Airy, S. C.; Sinsheimer, J. E. Isomerization of *trans*-Diethylstilbestrol to Pseudo-Diethylstilbestrol. *Steroids* **1981**, *38*, 593–603.

(25) Robertson, D. W.; Katzenellenbogen, J. A.; Long, D. J.; Rorke, E. A.; Katzenellenbogen, B. S.; Tamoxifen Antiestrogens, A. Comparison of the Activity, Pharmacokinetics, and Metabolic Activation of the Cis and Trans Isomers of Tamoxifen. *J. Steroid Biochem. Mol. Biol.* **1982**, *16*, 1–13.

(26) Murdter, T. E.; Schroth, W.; Bacchus-Gerybadze, L.; Winter, S.; Heinkele, G.; Simon, W.; Fasching, P. A.; Fehm, T.; Eichelbaum, M.;

Schwab, M.; Brauch, H. Activity Levels of Tamoxifen Metabolites at the Estrogen Receptor and the Impact of Genetic Polymorphisms of Phase I and II Enzymes on Their Concentration Levels in Plasma. *Clin. Pharmacol. Ther.* **2011**, *89*, 708−717.

(27) Lu, W. J.; Ferlito, V.; Xu, C.; Flockhart, D. A.; Caccamese, S. Enantiomers of Naringenin as Pleiotropic, Stereoselective Inhibitors of Cytochrome P450 Isoforms. *Chirality* **2011**, *23*, 891−896.